THE JOURNAL OF PHYSICAL CHEMISTRY B

Article

pubs.acs.org/JPCB

Ligand Binding to Heme Proteins: A Comparison of Cytochrome *c* Variants with Globins

Karin Nienhaus,[§] Franziska Zosel,[†] and G. Ulrich Nienhaus*[,§,‡]

[§]Institute of Applied Physics and Center for Functional Nanostructures (CFN), Karlsruhe Institute of Technology (KIT), Wolfgang-Gaede-Str. 1, D-76131 Karlsruhe, Germany

[†]Biochemical Institute, University Zürich, Winterthurerstrasse 190, CH-8057 Zürich, Switzerland

[‡]Department of Physics, University of Illinois at Urbana-Champaign, 1110 West Green Street, Urbana, Illinois 61801, United States

ABSTRACT: We have studied the binding of carbon monoxide (CO) in mutants of Cyt *c* having its methionine at position 80 replaced by alanine, aspartate, and arginine, so that the sixth coordination is available for ligand binding. We have employed Fourier transform infrared (FTIR) photolysis difference spectroscopy to examine interactions of the heme-bound and photolyzed CO (and also nitric oxide, NO) in the small heme pocket created by the mutations. By using FTIR temperature derivative spectroscopy (TDS) and nanosecond flash photolysis, the enthalpy barrier distributions for CO rebinding were determined. In flash photolysis experiments, the majority of ligands rebind to the heme iron on picosecond time scales so that only the high-barrier tail of the distributions is visible on the nanosecond scale. By continuous wave excitation prior to TDS characterization of the barriers, however, each Cyt *c* molecule is photoexcited multiple times and complete photodissociation can be achieved, which likely arises from a rotation of the CO within the heme pocket so that the oxygen faces the heme iron. Apparently, reorientation prior to rebinding constitutes an additional and significant contribution to the rebinding barrier. Our experiments reveal that the compact, rigid structure of Cyt *c* offers no alternative binding sites for photodissociated ligands in the protein matrix. A comparison of ligand binding in these Cyt *c* mutants and hemoglobins underscores the importance of internal ligand docking sites and ligand migration routes for conveying a ligand binding function to heme proteins.

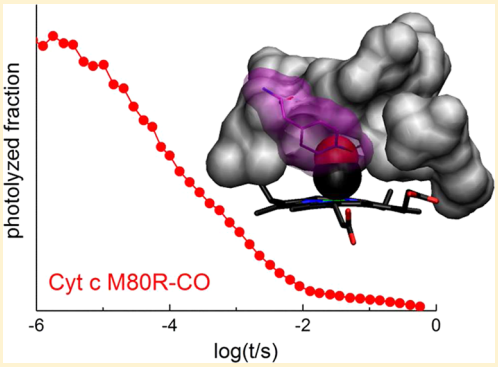

INTRODUCTION

Cytochrome *c* (Cyt *c*) is a small globular heme protein in the intermembrane space of mitochondria that carries electrons from the bc_1 complex to cytochrome *c* oxidase by means of a heme *c* prosthetic group covalently attached to Cys-14 and Cys-17 via thioether bonds. The heme iron is hexacoordinated to the four pyrrol nitrogens and His-18 and Met-80 as the axial ligands. Globins, by contrast, are a family of heme proteins that bind small diatomic ligands such as carbon monoxide (CO), dioxygen (O_2), and nitric oxide (NO) at the sixth coordination, because they either are pentacoordinate in the deligated state, such as myoglobin (Mb)[1−3] or hemoglobin (Hb),[4−6] or have a weakly bound endogenous ligand at the sixth coordination such as neuroglobin.[7,8] To imprint a similar ligand binding function into Cyt *c*, the Met-80 endogenous ligand can be removed from the heme iron, either by its carboxymethylation to yield carboxymethylated cytochrome *c* (CmCyt *c*)[9] or by genetic replacement by other amino acids.[10,11] The latter approach is not only more elegant but may also avoid altered protein−protein docking interfaces due to structural changes associated with carboxymethylation.

The vacant sixth coordination in the interior of the protein can bind small gaseous ligands such as CO. Figure 1 shows the active-site structure of Cyt *c* mutant M80A, as determined by X-ray crystallography,[12] together with the modeled structures of mutants M80D and M80R. The ability to bind ligands can be utilized for electron transfer studies, as exemplified by Brzezinski and Wilson[13] using CmCyt *c*: CO photolysis creates a five-coordinate ferrous heme, which is a good electron donor, so that its electron can be transferred to an acceptor, provided that the CO does not recombine too quickly. Geminate CO rebinding occurs on the picosecond time scale in the mutants shown in Figure 1,[14] and the yield of solvent escape is extremely small. Because the relevant electron transfer reactions are orders of magnitude slower, further engineering is required to develop variants in which the ligands are trapped away from the active site long enough for electron transfer to take place.

It is instructive to compare ligand binding in these Cyt *c* variants to globins such as Hb or Mb, which have been designed by evolution to reversibly bind gaseous ligands. Such a comparison may yield a better appreciation of the structure-dynamics-function relationships in these proteins in several ways. In globins, a flexible active-site structure is advantageous, as reorganization of the active site after ligand dissociation lowers the tendency to immediately recombine. In addition, specific ligand docking sites and entry/exit pathways have been

Received: July 9, 2012
Revised: August 28, 2012
Published: September 14, 2012

ACS Publications © 2012 American Chemical Society

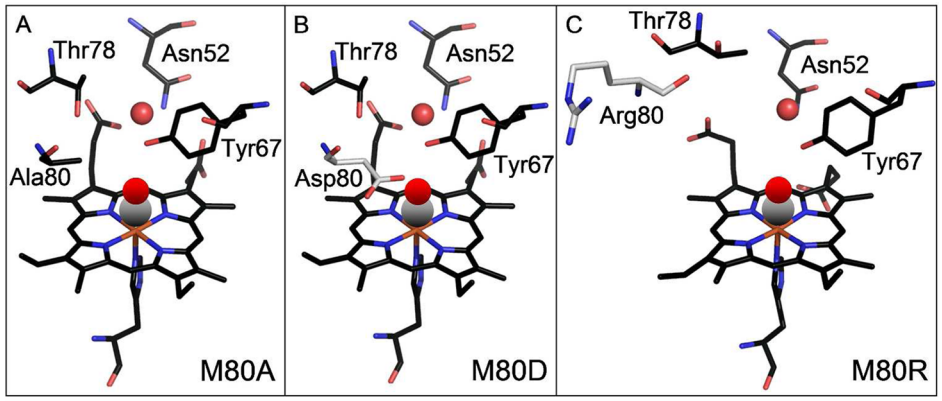

Figure 1. (A) Active site structure of yeast iso-1-Cyt *c* mutant M80A (pdb accession code 1FHB). The water molecule and the CO ligand have been superimposed onto the structure. (B, C) Possible active-site conformations of M80D and M80R, generated with the Pymol mutagenesis tool.

identified in globins that further increase the efficiency of ligand escape from the protein after bond cleavage.[15−19] By contrast, we expect markedly different properties for the Cyt *c* variants. For optimal function in electron transfer, the heme environment in cytochromes should be rather rigid so as to keep the reorganization energy small. This property is likely to result in extremely fast CO rebinding of the Cyt *c* mutants. Moreover, we anticipate that structural features facilitating ligand migration away from the active site to the exterior are entirely absent in Cyt *c*.

Here we have used Fourier transform infrared (FTIR) spectroscopy of the CO stretching vibration to investigate ligand binding and the possibility of ligand migration in Cyt *c* mutants at cryogenic temperatures. The high sensitivity of the CO stretching vibration to its electrostatic environment was utilized as a local probe that reports on active-site structural properties. We have also performed temperature derivative spectroscopy (TDS) experiments and nanosecond time-resolved flash photolysis experiments to assess the rebinding barriers at the heme iron. Indeed, ligand binding to Cyt *c* is markedly different from Mb, which points to the importance of other structural properties beyond a free heme coordination that are necessary for reversible ligand binding.

MATERIALS AND METHODS

Protein Expression. The DNA constructs coding for the mutant yeast iso-1-Cyt *c* proteins M80A, M80D, and M80R were kindly provided by Dr. G. Silkstone (University of Essex, Essex, U.K.). The DNA was freshly transformed and expressed in *E. coli* strain BL21 and purified as described.[10]

Fourier Transform Infrared (FTIR) Spectroscopy. Lyophilized Cyt *c* was dissolved in cryosolvent (75%/25% (v/v) glycerol/potassium phosphate buffer) to a final concentration of ∼10 mM, stirred under CO for 1 h, and reduced with a 2-fold molar excess of an anaerobically prepared sodium dithionite solution. The sample pH was measured at ambient temperature. FTIR transmission spectra were collected between 1800 and 2400 cm^{-1} at a resolution of 2 cm^{-1} using a FTIR spectrometer equipped with an InSb detector (IFS 66v/S, Bruker, Karlsruhe, Germany). Sample loading and cryospectroscopy equipment have been described previously.[15]

Temperature Derivative Spectroscopy. Temperature derivative spectroscopy (TDS) is a two-dimensional spectroscopic method that employs temperature as an additional parameter for studying thermally activated rate processes governed by enthalpy barrier distributions.[20,21] Prior to TDS data acquisition, a low temperature (typically, $T < 10$ K), nonequilibrium state is prepared by photolysis of the heme protein sample with visible light, and its relaxation back to equilibrium is subsequently recorded while the temperature is increased linearly in time over a few hours. An FTIR transmission spectrum, $I(\nu, T)$, is acquired every Kelvin. As the temperature is ramped up, rebinding occurs sequentially with respect to the heights of the enthalpy barriers that have to be surmounted in this process. In the simplest form of TDS data analysis, one assumes that a change in the integrated absorbance (spectral area) is solely due to recombination, so the absorbance change is set proportional to the rebinding population, $\Delta A(\nu, T) \propto \Delta N(\nu, T)$. Intrinsic temperature dependencies of the spectra, which may result from thermal fluctuations, can be taken into account by appropriate scaling.[22,23] The population changes between successive temperature steps are obtained by calculating absorbance difference spectra from transmission spectra at successive temperatures, $\Delta A(\nu, T) = \log[I(\nu, T - {}^1/_2\ \mathrm{K}) - I(\nu, T + {}^1/_2\ \mathrm{K})]$, which approximates the (negative) derivative of the population with respect to temperature, $-\mathrm{d}N(T)/\mathrm{d}T$. For a simple two-state reaction controlled by an enthalpy barrier, the distribution of barriers in the ensemble, $g(H)$, can be extracted from this quantity. TDS data are conveniently represented as two-dimensional contour plots of $-\mathrm{d}N(T)/\mathrm{d}T$ versus wavenumber and temperature, with black and red lines indicating an absorbance increase and decrease, respectively. Logarithmic spacing of the contour levels is used to emphasize small features.

Nanosecond Time-Resolved Spectroscopy. Low-temperature flash photolysis experiments were performed on dilute samples in 75%/25% glycerol/0.4 M potassium phosphate buffer, pH 8. Lyophilized protein was dissolved at a final concentration of ∼10 μM in the cryosolvent equilibrated with 5%/95% CO/N_2, followed by reduction with excess sodium dithionite solution. CO association kinetics was measured at 436 nm with our flash photolysis system.[24]

RESULTS

Photolysis Difference Spectra at 4 K. Samples were photodissociated by using two different illumination protocols. Either (i) the sample was illuminated for 10 s at 4 K or (ii) the sample was cooled from 160 to 4 K under constant laser illumination. In Mb and many other ligand binding globins,

dx.doi.org/10.1021/jp306775n | J. Phys. Chem. B 2012, 116, 12180−12188

brief illumination at 4 K results in trapping of the photolyzed CO predominantly at the primary docking site B close to the binding site,[25−27] whereas illumination during cooling enables the photodissociated ligands to sample alternative docking sites that may not be accessible at 4 K.[15,21,28] Photolysis-induced absorption difference spectra, $\Delta A(\nu, T)$, were then calculated from transmission spectra, $I(\nu, T)$, collected at 4 K before and after photolysis, $\Delta A(\nu, T) = \log(I_{dark}/I_{light})$.

The difference spectra of CO-ligated Cyt *c* obtained after brief illumination at 4 K are displayed in Figure 2. They are

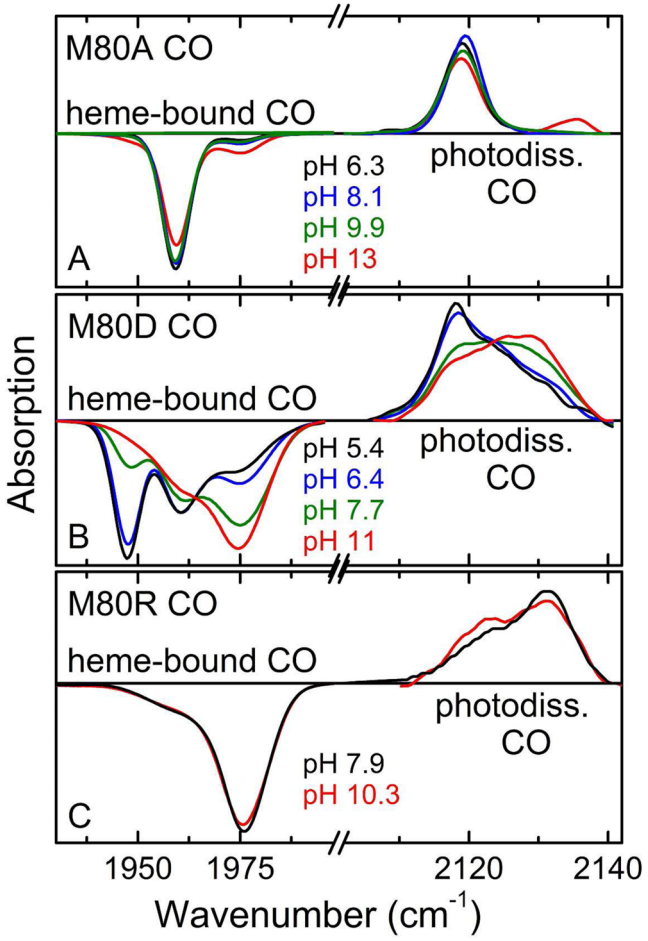

Figure 2. Photolysis difference spectra of ferrous CO-ligated (A) M80A, (B) M80D, and (C) M80R. Spectra have been scaled to equal areas.

absolutely identical to those determined after extended illumination (data not shown). The missing absorption of the heme-bound CO after photolysis is represented by the negative amplitudes of the so-called A bands in the range 1900−2000 cm^{-1}, and the newly emerging photoproduct, or B, bands (2100−2160 cm^{-1}) are depicted with positive amplitudes.[29−33] Peak positions and fractional occupancies were determined by fits with Gaussian band shapes; they are compiled in Table 1. For comparison, the difference spectra in each region were scaled to equal areas. The ratio between the A and B band areas is ∼35; it increases to 40 at pH 13 (for M80A).

Mutant M80A (Figure 2A) displays a dominant A band at 1959 cm^{-1} (A_{1959}) and a minor band at 1975 cm^{-1}. The spectrum is practically pH-independent in the range 6−12. At pH 13, the intensity of A_{1975} is increased at the expense of A_{1959}. The corresponding photoproduct spectra show a single peak at 2119 cm^{-1} (B_{2119}) at all pH values except pH 13, where a second band appears at 2135 cm^{-1}. In addition to the CO-ligated sample, we have also measured the photolysis difference spectrum of ferric NO-ligated M80A (data not shown). The A state spectrum looks like the spectrum of the CO-ligated form in Figure 2A, except that the bands are shifted by 39 cm^{-1} to 1920 cm^{-1} and 1936 cm^{-1}. The photolyzed NO gives rise to a very weak photoproduct band at 1856 cm^{-1}; the area in the B bands is ∼1/40 of that in the corresponding A state bands.

The photolysis difference spectra of M80D in Figure 2B reveal a pronounced pH dependence. There are three A state bands at 1948, 1961, and 1976 cm^{-1}; the low-frequency A_{1948} species dominates at low pH, whereas the broader high-frequency band A_{1976} is the largest one at high pH. Likewise, a systematic pH variation is observed in the photoproduct spectra, which can be modeled with three strongly overlapping bands at 2117, 2124, and 2131 cm^{-1}. Here, B_{2117} is the main band at low pH. From the change of the fractional occupancies of the A and B populations, it is apparent that B_{2117} and B_{2131} are the photoproduct bands of A_{1948} and A_{1976}, respectively.

In mutant M80R (Figure 2C), the absorption band of the heme-bound CO is centered on 1976 cm^{-1}, and a minority species exists at 1959 cm^{-1}, similar to M80A. However, the bands are broader and A_{1976} rather than A_{1959} is the dominant species. The photoproduct spectrum shows a doublet of bands at 2124 and 2132 cm^{-1} and is only weakly pH-dependent.

Temperature Derivative Spectroscopy. Immediately after sample illumination (either by brief illumination at 4 K or extended illumination during cooling), the light was switched off and TDS measurements were started. Select contour plots of the absorbance changes in the bands of heme-bound and photodissociated CO are presented in the left and right columns of Figure 3. The A state TDS map of M80A, pH 7.6, obtained after cooling under illumination from 160 to 4 K (Figure 3A) displays maximal rebinding in both A_{1959} and A_{1975} at 18 K, accompanied by the corresponding loss in the B_{2119} photoproduct band (Figure 3B). In addition, we observed a

Table 1. IR Stretching Frequencies of Heme-Bound and Photolyzed CO, Determined at 4 K

sample	pH	$\nu_{heme\text{-}bound\ CO}$ (cm^{-1})	fraction (%)	$\nu_{photodiss.\ CO}$ (cm^{-1})	fraction (%)
M80A	8.1	1959/1975	93/7	2119/−	100/−
	13.0		78/22	2119/2135	83/17
M80D	5.4	1948/1961/1976	38/34/28	2117/2124/2131	47/36/17
	6.4	1948/1961/1976	32/33/35	2117/2124/2131	43/37/20
	7.7	1948/1961/1976	13/30/57	2117/2124/2131	29/38/33
	11.0	1948/1961/1976	7/25/68	2117/2124/2131	23/36/41
M80R	7.9	1959/1976	13/87	2124/2132	
	10.1	1959/1976	13/87	2124/2132	

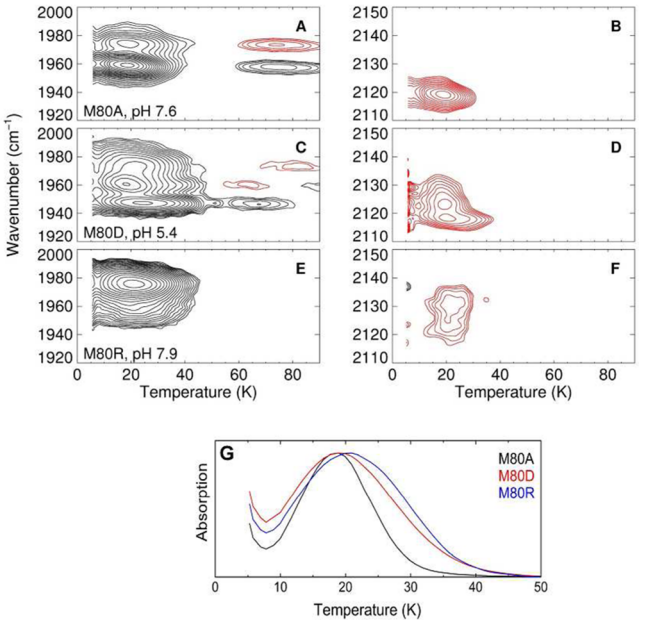

Figure 3. (A–F) TDS contour maps of Cyt *c* mutants, measured after cooling under illumination from 160 to 4 K. Left column: Absorption changes in the bands of heme-bound CO. Right column: Absorption changes in the photoproduct bands. Contours are spaced logarithmically; black and red lines represent increasing and decreasing absorption, respectively. (G) Temperature dependence of integrated absorption changes calculated from the TDS data in parts A, C, and E. The data were integrated over the entire spectral region of the A substate bands.

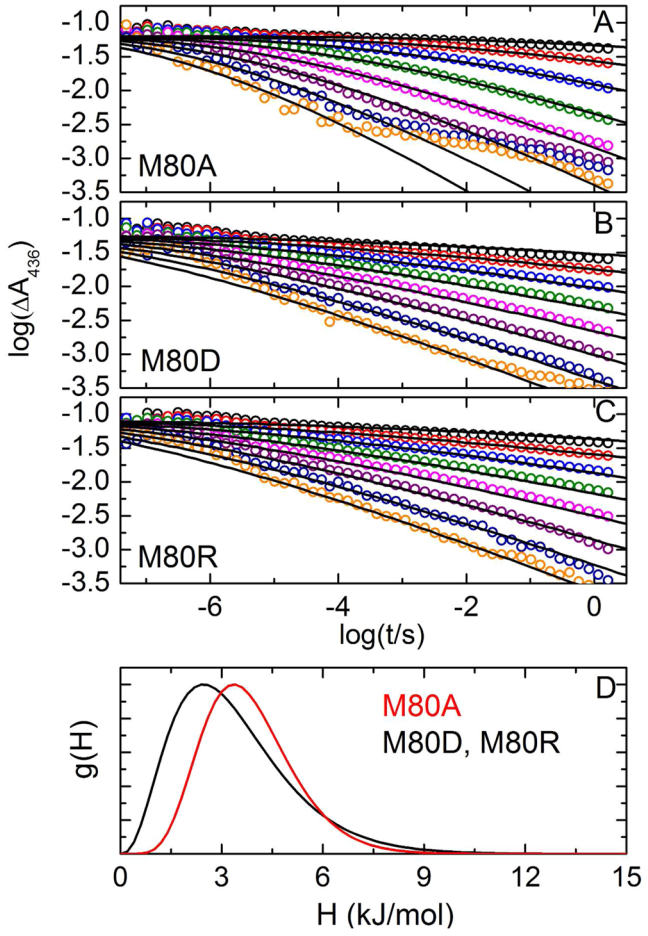

Figure 4. Recombination kinetics of (A) M80A, (B) M80D, and (C) M80R after 6 ns of illumination, monitored at 436 nm in the temperature range 15–50 K (in 5 K steps). Symbols are data; lines represent results from a global fit using eq 1. (D) g(*H*) distributions determined by the global fit of the data in parts A–C.

mirror image of black and red contours centered on 75 K in the A state map. A corresponding feature in the photoproduct map is absent, showing that these signals are not related to rebinding but rather indicate an exchange between heme-bound conformations. The TDS maps calculated after 20 s of illumination show the identical rebinding features (data not shown); the exchange is missing, however.

The TDS maps of mutant M80D after slow cooling under illumination are plotted in Figure 3C and D. Maximal recombination occurs at ∼20 K, with slight variations among the different conformations. As for M80A, a fairly complicated exchange pattern is visible between conformational substates in the pH 5.4 sample. The same pattern also appears in the TDS data of the pH 6.4 sample (data not shown), confirming its significance despite the rather weak signals. Again, brief illumination at 4 K results in essentially identical rebinding patterns (data not shown), but the exchange signals are absent.

The contour maps of mutant M80R (Figure 3E and F) also display maximal rebinding at ∼20 K; the exchange signature in the A state map is absent. For better comparison of the temperature dependence of ligand rebinding between the different samples, we present the absorbance changes integrated across the A state maps after brief illumination in Figure 3G, all scaled to equal amplitude.

Flash Photolysis at Cryogenic Temperatures. Dilute (∼10 μM) CO-ligated Cyt *c* mutant samples (pH 8) were photolyzed with a 6 ns laser flash at temperatures between 15 and 50 K. Ligand recombination was monitored at 436 nm from 30 ns to 1 s (Figure 4). At temperatures below the glass transition temperature of the cryosolvent (∼180 K), large-scale protein motions are arrested.[34,35] Therefore, ligands cannot exit from the protein, and only geminate rebinding occurs. The absorbance difference between a bound and a completely photodissociated sample can be estimated as ∼0.2 OD at the sample concentrations used, and the laser intensity should be sufficient for complete photodissociation. However, only ∼0.1 OD was observed at the earliest times, which indicates that only ∼50% of the sample is still photodissociated 100 ns after the flash. Within the time window of our experiment, there is a fast process ($t < 10$ μs) that is only weakly temperature dependent. This process, termed I*, observed earlier for CmCyt *c*,[36] protoheme,[37] and microperoxidase,[38,39] has a larger amplitude than the much slower, nonexponential geminate process extending over many orders of magnitude in time. At temperatures above 40 K and longer times ($t > 100$ μs), a third phase is observed for a tiny fraction (<1%) of molecules in M80A. Apart from this minor fraction, the temperature dependence of nonexponential rebinding is well described by a statically heterogeneous ensemble of molecules represented by a distribution of rebinding enthalpy barriers, $g(H)$, so that the fraction of hemes that is still unligated at time t after the flash, $N(t)$, is given by

$$N(t) = \int g(H)\, \exp[-k(H, T)\cdot t]\, dH \qquad (1)$$

Here, the measured absorbance change, $\Delta A(t)$, is taken to be proportional to $N(t)$. For thermally activated barrier crossing,

dx.doi.org/10.1021/jp306775n | J. Phys. Chem. B 2012, 116, 12180–12188

Table 2. Kinetic Parameters Describing CO Rebinding at Cryogenic Temperatures

	FTIR/TDS			flash photolysis		
	log (A/s^{-1})	H_{peak} (kJ/mol)	σ (kJ/mol)	log (A/s^{-1})[a]	H_{peak}[a] (kJ/mol)	α (kJ/mol)
M80A	10.7	4.3 ± 0.006	1.4 ± 0.002	10.9 ± 0.3	3.4 ± 0.5	2.1
M80D	10.7	4.6 ± 0.012	2.1 ± 0.007	10.9 ± 0.3	2.5 ± 0.2	1.14
M80R	10.7	4.8 ± 0.004	2.2 ± 0.004	10.9 ± 0.3	2.5 ± 0.3	1.14

[a]Errors reflect a 50% increase in χ^2.

the rebinding rate coefficient, $k(H, T)$, is given by the transition state expression

$$k(H, T) = A\frac{T}{T_0}\exp\left[-\frac{H}{RT}\right] \quad (2)$$

with pre-exponential factor A, reference temperature T_0 set to 100 K, and the universal gas constant R. We have fitted the kinetics globally with eqs 1 and 2, using a gamma function,

$$\Gamma(H) \propto (H - H_{min})^{\alpha(H_{peak}-H_{min})}\exp[-\alpha(H - H_{min})] \quad (3)$$

as a model distribution (Figure 4).[40,41] This asymmetric distribution is characterized by the parameters H_{min}, H_{peak}, and α, which represent the lower enthalpy cutoff (which was set to 10^{-3} kJ/mol), the peak enthalpy, and the width parameter, respectively. The resulting distributions are plotted in Figure 4D; the fit parameters are summarized in Table 2. All three distributions are similar, and M80D and M80R are described by identical distributions within the statistics of the data.

Formation and Yield of Photoproducts. Comparison of the FTIR and flash photolysis data poses a conundrum: How can we achieve rather complete (80−90%) and long-lived photodissociation with our FTIR samples if the large majority rebinds in flash photolysis experiments with lifetimes of less than 10 μs? To clarify this issue, we have studied photodissociation on a mixed sample, containing both CO derivatives of Cyt *c* M80A and Mb mutant L29F using FTIR spectroscopy at 5 K. The L29F Mb variant was chosen because it forms an extremely slowly rebinding photoproduct at 5 K, and its CO stretching vibration is spectrally completely separated from the one of M80A. The light from the photolysis laser was attenuated 1000-fold by using a 3-OD neutral density filter. Figure 5A shows the photodissociated species increasing over the time course of 25 000 s. For the Mb variant, the 1/*e* point toward saturation is reached after 45 s, which would correspond to 45 ms without filter, i.e., at full power. For Cyt *c*, a pronounced sigmoidal shape is obtained that reaches its 1/*e* point much more slowly, namely, at ∼250 s. From comparing the responses of the two proteins, we conclude that the Cyt *c* molecules have roughly experienced ∼5 photolysis events before they assumed a photoproduct state with a lifetime longer than the experimental scale of 25 000 s. Immediately after illumination, we measured rebinding in the dark (Figure 5B). Whereas it is easier to photolyze L29F MbCO, rebinding is much faster in this protein, in agreement with its lower peak rebinding temperature in the TDS contour plot in Figure 5C.

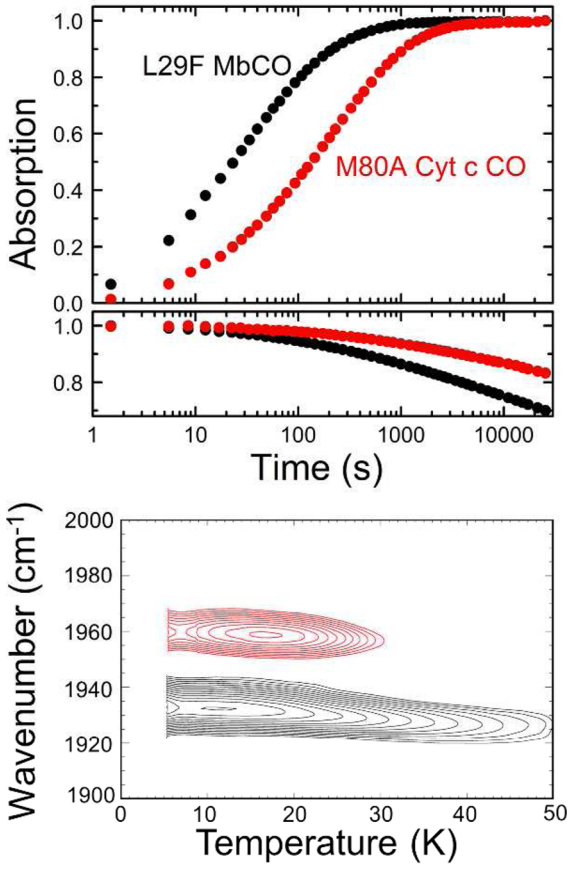

Figure 5. (A) Photolysis yields of L29F MbCO (black symbols) and CO-ligated M80A Cyt *c* (red symbols) upon constant laser illumination through a 3-OD neutral density filter at 4 K, calculated from the decrease of the absorption bands of the heme-bound ligand. (B) Relaxation of the photolyzed states prepared in part A toward the bound state after switching off the illumination light. (C) TDS contour map showing the absorption increases in the bands of heme-bound CO due to rebinding. The sample was photolyzed for 1 s at 4 K through a 0.7 OD neutral density filter. Red: M80A Cyt *c*. Black: L29F Mb.

DISCUSSION

Structural Heterogeneity at the Active Sites of Cyt *c* Variants. The polypeptide chain of Cyt *c* forms a hydrophobic pocket to accommodate its heme prosthetic group.[42] The charged heme propionates are buried within the protein matrix, forming multiple hydrogen bonds with surrounding residues. Overall, the protein is densely packed; only a single internal cavity can be identified using a probe sphere with a radius of 1.4 Å.[42] The most rigid parts of the protein are close to the heme group so as to minimize the reorganization energy during electron transfer.

Currently, from the three Cyt *c* mutants studied in this work, there is only an X-ray structure of CN^--ligated M80A (pdb accession code 1FHB) available.[12] The FTIR difference spectra presented here allow us to pinpoint key structural properties of the M80D and M80R mutants and to assess conformational heterogeneity that usually can be detected by X-ray crystallography only at very high resolution. To this end, we have exploited the exquisite sensitivity of the strong CO (and

NO) stretching absorption bands to their environment, which is based on electrostatic interactions, also known as the vibrational Stark effect.[22,43−48] When bound in the active site of heme proteins, these ligands frequently display multiple absorption bands, indicating discrete active-site structures.[49,50] Positive (negative) partial charges placed near the oxygen atom of the bound CO shift the stretching frequency to lower (higher) values. This phenomenon has been explained by the backbonding model.[51−53] After photodissociation from the heme iron, CO reorientation and/or migration to other sites may occur, which can also be monitored via the stretching spectra of the photodissociated CO within the protein. Cyt *c* mutant M80A has a dominant CO stretching band at 1959 cm^{-1} and a minor one at 1975 cm^{-1}. The spectrum remains constant over a wide pH range (Figure 2A). A CO stretching frequency of 1965 cm^{-1} is typically observed for those Mb mutants for which the CO has a negligible interaction with the distal environment.[49,50] The lower stretching frequency of 1959 cm^{-1} in Cyt *c* M80A indicates a comparatively weak interaction with a positive partial charge, for example, a hydrogen atom. Tyr-67 is the amino acid closest to the heme-bound ligand; its hydroxyl proton interacts with the sulfur of Met-80 in the native protein. On the basis of the X-ray structure of CN^--ligated M80A,[12] the distance between the Tyr-67 hydroxyl group and the CO oxygen is ∼3.2 Å (Figure 1A), which suggests that a weak hydrogen-bond between the Tyr-67 hydroxyl and the heme-bound CO could be responsible for the slightly red-shifted stretching frequency of 1959 cm^{-1}. In contrast, the high frequency of the minority species at 1975 cm^{-1} implies that a negative partial charge interacts with the CO transition dipole. This interaction can be provided by the lone pair on the Tyr-67 hydroxyl oxygen if it is not hydrogen-bonded to the ligand. In native Cyt *c*, a water molecule (Wat-166) forms hydrogen bonds to Asn-52, Tyr-67, and Thr-78 (Figure 1A), which helps to maintain the conformation of the Tyr-67 side chain and also provides a convenient mechanism to modify the hydrogen bonding network.[54] The complementary positive and negative features above 60 K in the TDS contour plot in Figure 3A reveal that the two substates exchange population in this temperature range. In heme proteins, exchanges of A band populations are rarely observed at such low temperatures, as they typically involve major conformational rearrangements that are completely arrested below ∼180 K.[55] Only fairly localized reorientations are possible, such as rearrangements within a hydrogen bonding network, which have been invoked earlier to explain similar effects in *Cerebratulus lacteus* Hb.[56] As a consequence of such a change in hydrogen bonding, the Tyr-67 hydroxyl may switch between pointing its oxygen lone pair or its hydrogen toward the ligand. This hypothesis is further supported by the spectrum at pH 13 in Figure 2A. At high pH, the fraction of deprotonated Tyr-67 side chains increases, which leads to a concomitant increase of the high-frequency species at 1975 cm^{-1}.

Ferric NO-ligated M80A displays absorption bands at 1920 and 1936 cm^{-1}. The NO spectrum looks essentially like the CO spectrum down-shifted by 39 cm^{-1}. As ferrous CO-ligated Cyt *c* is isoelectronic to ferric NO-ligated Cyt *c*, we suggest that the different frequencies also arise from the different hydrogen bonding interactions between the NO and the Tyr-67 side chain. This interpretation is further supported by results with ferric MbNO, in which three A substate bands appear due to different interactions with a lone-pair orbital on the deprotonated His-64 Nδ.[57]

In mutant M80D of Cyt *c*, a CO stretching band appears at 1948 cm^{-1} in addition to the two bands at 1961 and 1976 cm^{-1}, which have similar frequencies as those already reported for M80A. The much lower frequency of the additional band indicates a significant interaction of the CO with a positive partial charge in its vicinity. Moreover, M80D displays a pronounced pH dependence of the A substate spectrum from pH 5 to 11 (Figure 2B). The isosbestic point in this series of spectra implies protonation of a single group, presumably Asp-80 itself. Apparently, the high-frequency band at 1976 cm^{-1} represents the basic form and the other two bands the acidic form. The TDS contour plot in Figure 3D reveals that all three substates are involved in population exchanges occurring between 50 and 100 K. As already discussed above, major orientational changes of the Asp-80 side chain in M80D, e.g., pointing toward the binding site in one conformation and toward the solvent in another one, can be safely excluded as an explanation of the observed structural heterogeneity. The similarity of the M80A and M80D (and M80R, see below) spectra also suggests that a direct interaction between the bound ligand and the Asp-80 carbonyl is rather unlikely, but further details cannot be revealed from these results.

In M80R, there are again two bands at similar positions as in M80A and M80D, at 1959 and 1976 cm^{-1} (Figure 2C). In contrast to M80D, there is essentially no systematic change with pH, and the high-frequency band dominates the spectrum. The similar CO stretching spectrum in M80R, despite the introduction of a positively charged and very bulky side chain, strongly suggests that the guanidino group does not reside inside the distal pocket near the heme-bound CO but rather points into the solvent to solvate its charge. In fact, it is not possible to replace Ala-80 by Arg-80 in the X-ray structure of the M80A mutant without producing severe steric clashes; additional, large-scale structural changes are required. For the native protein, it was shown that cyanide binding to the ferric form caused the loop consisting of residues 77−85 to swing out and widen the heme crevice.[58] A model of a possible M80R mutant based on this structure (pdb accession code 1I5T) is plotted in Figure 1C. A possible explanation for the preferred high-frequency conformation could be a higher occupancy of the water molecule inside the heme pocket.

Ligand Trapping within the Protein. The spectrum of photodissociated CO in M80A displays a dominant photoproduct band at 2119 cm^{-1} which is, therefore, assigned to the photoproduct of the dominant A substate band at 1959 cm^{-1}. Only at pH 13 can we clearly detect a second photoproduct band at 2135 cm^{-1}, which is associated with the high-frequency A state band at 1975 cm^{-1}. Such a mapping between bound and photoproduct states indicates that the CO remains close to the active site after photolysis so that it experiences the structural differences seen in the bound-state spectra also in the photoproduct. In MbCO, CO in the primary photoproduct site displays two bands at 2119 and 2131 cm^{-1} that arise from vibrational Stark splitting between two opposing orientations of the CO in this site.[59−61] The fact that we find only one photoproduct band for each A substate band in Cyt *c* M80A suggests that those CO molecules that stay photodissociated on the experimental time scale (∼100 s) can only assume a single orientation. In MbCO, the lower frequency of 2119 cm^{-1} was assigned to that orientation of the CO in which the oxygen points toward the heme iron. In Cyt *c*, the CO presumably points with its oxygen toward the heme iron. In M80D, the photoproduct spectra show multiple bands and a pronounced

pH dependence that was already observed for the A substate bands. The mapping between the A and B substates shows, as for M80A, that the CO experiences the active-site structural heterogeneity also in the photoproduct bands. The photoproduct spectra of M80R lend further support to this notion.

Ligand Migration and Rebinding at Cryogenic Temperatures. In Mb[24,57] and other globular heme proteins,[56,62−64] extended illumination during cooling from 160 to 4 K leads to efficient migration of CO or NO ligands to secondary docking sites with modified photoproduct spectra and altered rebinding barriers. Both spectroscopy and (time-resolved) X-ray crystallography studies have emphasized the importance of these docking sites for ligand binding to globins.[16,65−71] Within picoseconds after dissociation from the heme iron, ligands move to the primary docking site B in the distal heme pocket, which plays a key role in iron−ligand bond formation. This unique site is engineered such that ligands can reside there for nanoseconds without rebinding. In addition, ligands shuttle back and forth between the primary docking site and secondary sites, which further reduces their probability of rebinding while they wait for large-scale protein fluctuations on nanosecond to microsecond time scales that open exit channels through which the ligands finally escape from the protein.[15,16,24,69]

There are, however, other mechanisms to promote ligand release from the heme iron. The lipocalin β-barrel of the NO transporting heme protein in the bloodsucking insect *Rhodnius prolixus*, NP4, does not provide secondary transient ligand docking sites in the interior of the protein that could support ligand escape after thermal dissociation from the heme iron. Instead, NP4 has developed a unique mechanism that relies on a protein conformational change.[23] In the closed, low-pH conformation, ligand escape from the active site of NP4 is prevented by an extremely reactive heme iron and the absence of secondary ligand docking sites. In the open, high-pH conformation, ligand escape is facilitated, and blockage of the active site by water hinders reassociation of NO to the ferric (Fe^{3+}) heme iron.

In all three Cyt *c* mutants, slow-cool illumination does not affect the photoproduct spectra, indicating that secondary docking sites are completely absent. The TDS data of the mutant Cyt *c* samples recorded after extended illumination from 160 to 4 K (Figure 3) show the identical photoproduct bands and temperature dependences of rebinding as 1 s of illumination at 4 K, confirming that the CO is entirely unable to migrate or to change its conformation within the distal heme pocket of the mutants. The only difference between the two photolysis protocols is the exchange in the A substates in M80A and M80D, which only occurs under extended illumination. These findings confirm our expectation that Cyt *c* forms a rather tight protein matrix void of any free space to transiently store small ligands or to allow their passage.

Photoproduct and heme-bound states are separated by an enthalpy barrier against recombination, *H*. At cryogenic temperatures, each protein molecule is frozen in a slightly different conformation, as indicated by a distribution of barrier heights, $g(H)$, that characterizes the ensemble of protein molecules.[1,3,72] Rebinding from the primary docking sites in the Cyt *c* samples stretches from 4 to 40 K; it is maximal at ∼20 K (Figure 3). With an Arrhenius prefactor of $10^{10.7}$ s^{-1} determined from a global fit of the rebinding traces (Figure 4) to eqs 1 and 2, the enthalpy barrier distributions were determined from the TDS data peak at ∼4−5 kJ/mol (Figure 3D, Table 2), whereas the $g(H)$ distributions obtained from a global fit of the flash photolysis data (Figure 4) yield significantly lower barrier peaking at 3.4 kJ/mol for M80A and 2.5 kJ/mol for the other two mutants (Table 2). Moreover, at early times ($t < 10^{-6}$ s), the kinetic traces deviate systematically from the fit for all three mutants, indicating an even faster rebinding fraction of ligands with lower enthalpy barriers. This fraction presumably comprises CO molecules that point their C atom toward the heme iron. For M80A, rebinding is slower than predicted at long times and higher temperatures (Figure 4A). We note that this process involves less than 1% of the entire population so that it goes undetected in the FTIR/TDS experiment. Such an effect is often seen in flash photolysis data taken on heme proteins and may indicate either heme iron out-of-plane relaxation or ligand trapping in other docking sites with a higher enthalpy barrier against rebinding.[3,73,74]

The observed differences in the heights of the enthalpy barriers between the TDS and flash photolysis data may result from the fact that the photodissociated ensemble is prepared in an entirely different way. A nanosecond laser flash gives rise to only a single photon absorption event in the majority of protein molecules, whereas the longer duration of the photodissociation with a continuous-wave laser in the TDS experiment makes multiple photoexcitation events more likely. In fact, we have observed that the rebinding kinetics slow with increasing continuous-wave photolysis laser powers (1−10 s exposure, data not shown). The data in Figure 5 have shown that those Cyt *c* photoproduct molecules that are observed with the TDS method have experienced multiple photoexcitation events, which may enhance the probability that the CO ligands rotate within a rather tight space in the immediate vicinity of the binding site. If the ligand oxygen points at the heme iron, the CO has to first rotate to rebind the heme iron. In MbCO, the barrier against rotation in site B has been determined as 3−4 kJ/mol,[32,59] which is comparable the differences discussed here. Those CO molecules that settle in site B with the carbon atom pointing at the heme iron will be much more reactive and likely rebind on time scales that are not even accessible with nanosecond flash photolysis.

■ CONCLUSIONS

In their pioneering work of 1975, Frauenfelder and co-workers[1] found a bewildering complexity in the apparently "simple" biological process of ligand binding to Mb. Over the last four decades, much of this complexity has been firmly understood. Globins possess internal cavities that provide transient ligand storage sites. Ligands can reside in these sites for several hundred nanoseconds after dissociation from the heme iron, so that large-scale fluctuations open pathways for ligand escape.[17,24,64,75] Ligand entry and exit may occur either by a simple fluctuating gate[16,64,76,77] or by more complicated structural features such as a specific tunnel in *Cerebratulus lacteus* Hb.[28,78] Besides docking sites and ligand migration pathways, occlusion of the binding site by distal pocket residues, most importantly, His64, and the ability of the heme group to relax into its pentacoordinate form after ligand dissociation are further important mechanisms that control ligand affinity and kinetics.[3,5,79]

In contrast, ligand binding to Cyt *c* mutants with an engineered cavity is extremely fast even at very low temperatures because of small enthalpy barriers against rebinding. These arise because the rigid Cyt *c* structure allows only minimal reorganization, and there are no residues hindering

ligand access to the heme iron. Importantly, the protein matrix is dense and does not provide internal ligand docking sites such as the primary (B) site near the heme iron and secondary sites. It will be interesting to see how ligand binding will be affected by further modified Cyt *c* providing more internal space for ligand movement.

AUTHOR INFORMATION

Corresponding Author

*E-mail: uli@uiuc.edu.

Notes

The authors declare no competing financial interest.

ACKNOWLEDGMENTS

This work was supported by the Deutsche Forschungsgemeinschaft (DFG, grants Ni 291/10 and CFN). The plasmids were kindly provided by Dr. G. Silkstone (University of Essex, Essex, U.K.). We thank Uwe Theilen for expression and purification of the recombinant proteins used in this study.

DEDICATION

This work is dedicated to Professor Hans Frauenfelder on the occasion of his 90th birthday. With his many seminal contributions, he paved the road toward a detailed atomic-level understanding of ligand binding and protein dynamics.

REFERENCES

(1) Austin, R. H.; Beeson, K. W.; Eisenstein, L.; Frauenfelder, H.; Gunsalus, I. C. *Biochemistry* **1975**, *14*, 5355−5373.
(2) Henry, E. R.; Sommer, J. H.; Hofrichter, J.; Eaton, W. A. *J. Mol. Biol.* **1983**, *166*, 443−451.
(3) Steinbach, P. J.; Ansari, A.; Berendzen, J.; Braunstein, D.; Chu, K.; Cowen, B. R.; Ehrenstein, D.; Frauenfelder, H.; Johnson, J. B.; Lamb, D. C.; et al. *Biochemistry* **1991**, *30*, 3988−4001.
(4) Eaton, W. A.; Henry, E. R.; Hofrichter, J.; Mozzarelli, A. *Nat. Struct. Biol.* **1999**, *6*, 351−358.
(5) Friedman, J. M. *Science* **1985**, *228*, 1273−1280.
(6) Perutz, M. F. *Nature* **1970**, *228*, 726−739.
(7) Brunori, M.; Giuffre, A.; Nienhaus, K.; Nienhaus, G. U.; Scandurra, F. M.; Vallone, B. *Proc. Natl. Acad. Sci. U.S.A.* **2005**, *102*, 8483−8488.
(8) Nienhaus, K.; Kriegl, J. M.; Nienhaus, G. U. *J. Biol. Chem.* **2004**, *279*, 22944−22952.
(9) Schejter, A.; George, P. *Nature* **1965**, *206*, 1150−1151.
(10) Silkstone, G.; Stanway, G.; Brzezinski, P.; Wilson, M. T. *Biophys. Chem.* **2002**, *98*, 65−77.
(11) Silkstone, G.; Stanway, G.; Wilson, M. T. *Biochem. Soc. Trans.* **1998**, *26*, S348.
(12) Banci, L.; Bertini, I.; Bren, K. L.; Gray, H. B.; Sompornpisut, P.; Turano, P. *Biochemistry* **1995**, *34*, 11385−11398.
(13) Brzezinski, P.; Wilson, M. T. *Proc. Natl. Acad. Sci. U.S.A.* **1997**, *94*, 6176−6179.
(14) Silkstone, G.; Jasaitis, A.; Wilson, M. T.; Vos, M. H. *J. Biol. Chem.* **2007**, *282*, 1638−1649.
(15) Nienhaus, K.; Deng, P.; Kriegl, J. M.; Nienhaus, G. U. *Biochemistry* **2003**, *42*, 9633−9646.
(16) Schmidt, M.; Nienhaus, K.; Pahl, R.; Krasselt, A.; Anderson, S.; Parak, F.; Nienhaus, G. U.; Srajer, V. *Proc. Natl. Acad. Sci. U.S.A.* **2005**, *102*, 11704−11709.
(17) Brunori, M.; Gibson, Q. H. *EMBO Rep.* **2001**, *2*, 674−679.
(18) Tilton, R. F., Jr.; Kuntz, I. D., Jr.; Petsko, G. A. *Biochemistry* **1984**, *23*, 2849−2857.
(19) Scott, E. E.; Gibson, Q. H. *Biochemistry* **1997**, *36*, 11909−11917.
(20) Berendzen, J.; Braunstein, D. *Proc. Natl. Acad. Sci. U.S.A.* **1990**, *87*, 1−5.
(21) Chu, K.; Ernst, R. M.; Frauenfelder, H.; Mourant, J. R.; Nienhaus, G. U.; Philipp, R. *Phys. Rev. Lett.* **1995**, *74*, 2607−2610.
(22) Kriegl, J. M.; Nienhaus, K.; Deng, P.; Fuchs, J.; Nienhaus, G. U. *Proc. Natl. Acad. Sci. U.S.A.* **2003**, *100*, 7069−7074.
(23) Nienhaus, K.; Maes, E. M.; Weichsel, A.; Montfort, W. R.; Nienhaus, G. U. *J. Biol. Chem.* **2004**, *279*, 39401−39407.
(24) Nienhaus, K.; Deng, P.; Kriegl, J. M.; Nienhaus, G. U. *Biochemistry* **2003**, *42*, 9647−9658.
(25) Hartmann, H.; Zinser, S.; Komninos, P.; Schneider, R. T.; Nienhaus, G. U.; Parak, F. *Proc. Natl. Acad. Sci. U.S.A.* **1996**, *93*, 7013−7016.
(26) Schlichting, I.; Berendzen, J.; Phillips, G. N., Jr.; Sweet, R. M. *Nature* **1994**, *371*, 808−812.
(27) Teng, T. Y.; Srajer, V.; Moffat, K. *Nat. Struct. Biol.* **1994**, *1*, 701−705.
(28) Salter, M. D.; Nienhaus, K.; Nienhaus, G. U.; Dewilde, S.; Moens, L.; Pesce, A.; Nardini, M.; Bolognesi, M.; Olson, J. S. *J. Biol. Chem.* **2008**, *283*, 35689−35702.
(29) Shimada, H.; Caughey, W. S. *J. Biol. Chem.* **1982**, *257*, 11893−11900.
(30) Fuchsman, W. H.; Appleby, C. A. *Biochemistry* **1979**, *18*, 1309−1321.
(31) Mourant, J. R.; Braunstein, D. P.; Chu, K.; Frauenfelder, H.; Nienhaus, G. U.; Ormos, P.; Young, R. D. *Biophys. J.* **1993**, *65*, 1496−1507.
(32) Alben, J. O.; Beece, D.; Bowne, S. F.; Doster, W.; Eisenstein, L.; Frauenfelder, H.; Good, D.; McDonald, J. D.; Marden, M. C.; Moh, P. P.; et al. *Proc. Natl. Acad. Sci. U.S.A.* **1982**, *79*, 3744−3748.
(33) Polack, T.; Ogilvie, J. P.; Franzen, S.; Vos, M. H.; Joffre, M.; Martin, J. L.; Alexandrou, A. *Phys. Rev. Lett.* **2004**, *93*, 018102.
(34) Nienhaus, G. U.; Heinzl, J.; Huenges, E.; Parak, F. *Nature* **1989**, *338*, 665−666.
(35) Frauenfelder, H.; Nienhaus, G. U.; Johnson, J. B. *Ber. Bunsen-Ges. Phys. Chem.* **1991**, *95*, 272−278.
(36) Alberding, N.; Austin, R. H.; Chan, S. S.; Eisenstein, L.; Frauenfelder, H.; Good, D.; Kaufmann, K.; Marden, M.; Nordlund, T. M.; Reinisch, L.; et al. *Biophys. J.* **1978**, *24*, 319−334.
(37) Postlewaite, J. C.; Miers, J. B.; Dlott, D. D. *J. Am. Chem. Soc.* **1989**, 1248−1255.
(38) Cao, W.; Ye, X.; Georgiev, G. Y.; Berezhna, S.; Sjodin, T.; Demidov, A. A.; Wang, W.; Sage, J. T.; Champion, P. M. *Biochemistry* **2004**, *43*, 7017−7027.
(39) Lim, M.; Jackson, T. A.; Anfinrud, P. A. *J. Biol. Inorg. Chem.* **1997**, *2*, 531−536.
(40) Young, R. D.; Bowne, S. F. *J. Chem. Phys.* **1984**, *81*, 3730−3737.
(41) Lamb, D. C.; Prusakov, V.; Engler, N.; Ostermann, A.; Schellenberg, P.; Parak, F. G.; Nienhaus, G. U. *J. Am. Chem. Soc.* **1998**, *120*, 2981−2982.
(42) Louie, G. V.; Brayer, G. D. *J. Mol. Biol.* **1990**, *214*, 527−555.
(43) Bishop, D. M. *J. Chem. Phys.* **1993**, *98*, 3179−3184.
(44) Hush, N. S.; Reimers, J. R. *J. Phys. Chem.* **1995**, *99*, 15798−15805.
(45) Park, E. S.; Andrews, S. S.; Hu, R. B.; Boxer, S. G. *J. Phys. Chem. B* **1999**, *103*, 9813−9817.
(46) Park, E. S.; Boxer, S. G. *J. Phys. Chem. B* **2002**, *106*, 5800−5806.
(47) Lehle, H.; Kriegl, J. M.; Nienhaus, K.; Deng, P.; Fengler, S.; Nienhaus, G. U. *Biophys. J.* **2005**, *88*, 1978−1990.
(48) Phillips, G. N., Jr.; Teodoro, M. L.; Li, T.; Smith, B.; Olson, J. S. *J. Phys. Chem. B* **1999**, *103*, 8817−8829.
(49) Li, T.; Quillin, M. L.; Phillips, G. N., Jr.; Olson, J. S. *Biochemistry* **1994**, *33*, 1433−1446.
(50) Braunstein, D. P.; Chu, K.; Egeberg, K. D.; Frauenfelder, H.; Mourant, J. R.; Nienhaus, G. U.; Ormos, P.; Sligar, S. G.; Springer, B. A.; Young, R. D. *Biophys. J.* **1993**, *65*, 2447−2454.
(51) Li, X. Y.; Spiro, T. G. *J. Am. Chem. Soc.* **1988**, *110*, 6024−6033.
(52) Vogel, K. M.; Kozlowski, P. M.; Zgierski, M. Z.; Spiro, T. G. *J. Am. Chem. Soc.* **1999**, *121*, 9915−9921.
(53) Ray, G. B.; Li, X.-Y.; Ibers, J. A.; Sessler, J. L.; Spiro, G. S. *J. Am. Chem. Soc.* **1994**, *116*, 162−176.

(54) Berghuis, A. M.; Guillemette, J. G.; McLendon, G.; Sherman, F.; Smith, M.; Brayer, G. D. *J. Mol. Biol.* **1994**, *236*, 786−799.
(55) Parak, F. G.; Nienhaus, G. U. *ChemPhysChem* **2002**, *3*, 249−254.
(56) Deng, P.; Nienhaus, K.; Palladino, P.; Olson, J. S.; Blouin, G.; Moens, L.; Dewilde, S.; Geuens, E.; Nienhaus, G. U. *Gene* **2007**, *398*, 208−223.
(57) Nienhaus, K.; Palladino, P.; Nienhaus, G. U. *Biochemistry* **2008**, *47*, 935−948.
(58) Yao, Y.; Qian, C.; Ye, K.; Wang, J.; Bai, Z.; Tang, W. *J. Biol. Inorg. Chem.* **2002**, *7*, 539−547.
(59) Nienhaus, K.; Olson, J. S.; Franzen, S.; Nienhaus, G. U. *J. Am. Chem. Soc.* **2005**, *127*, 40−41.
(60) Bredenbeck, J.; Helbing, J.; Nienhaus, K.; Nienhaus, G. U.; Hamm, P. *Proc. Natl. Acad. Sci. U.S.A.* **2007**, *104*, 14243−14248.
(61) Lim, M.; Jackson, T. A.; Anfinrud, P. A. *Nat. Struct. Biol.* **1997**, *4*, 209−214.
(62) Lutz, S.; Nienhaus, K.; Nienhaus, G. U.; Meuwly, M. *J. Phys. Chem. B* **2009**, *113*, 15334−15343.
(63) Nienhaus, K.; Dominic, P.; Astegno, A.; Abbruzzetti, S.; Viappiani, C.; Nienhaus, G. U. *Biochemistry* **2010**, *49*, 7448−7458.
(64) Nienhaus, K.; Knapp, J. E.; Palladino, P.; Royer, W. E., Jr.; Nienhaus, G. U. *Biochemistry* **2007**, *46*, 14018−14031.
(65) Schotte, F.; Lim, M.; Jackson, T. A.; Smirnov, A. V.; Soman, J.; Olson, J. S.; Phillips, G. N., Jr.; Wulff, M.; Anfinrud, P. A. *Science* **2003**, *300*, 1944−1947.
(66) Hummer, G.; Schotte, F.; Anfinrud, P. A. *Proc. Natl. Acad. Sci. U.S.A.* **2004**, *101*, 15330−15334.
(67) Findsen, E. W.; Friedman, J. M.; Ondrias, M. R.; Simon, S. R. *Science* **1985**, *229*, 661−665.
(68) Bourgeois, D.; Vallone, B.; Schotte, F.; Arcovito, A.; Miele, A. E.; Sciara, G.; Wulff, M.; Anfinrud, P.; Brunori, M. *Proc. Natl. Acad. Sci. U.S.A.* **2003**, *100*, 8704−8709.
(69) Nienhaus, K.; Ostermann, A.; Nienhaus, G. U.; Parak, F. G.; Schmidt, M. *Biochemistry* **2005**, *44*, 5095−5105.
(70) Srajer, V.; Ren, Z.; Teng, T. Y.; Schmidt, M.; Ursby, T.; Bourgeois, D.; Pradervand, C.; Schildkamp, W.; Wulff, M.; Moffat, K. *Biochemistry* **2001**, *40*, 13802−13815.
(71) Anfinrud, P. A.; Han, C.; Hochstrasser, R. M. *Proc. Natl. Acad. Sci. U.S.A.* **1989**, *86*, 8387−8391.
(72) Nienhaus, G. U.; Müller, J. D.; McMahon, B. H.; Frauenfelder, H. *Physica D* **1997**, *107*, 297−311.
(73) Ostermann, A.; Waschipky, R.; Parak, F. G.; Nienhaus, G. U. *Nature* **2000**, *404*, 205−208.
(74) Johnson, J. B.; Lamb, D. C.; Frauenfelder, H.; Müller, J. D.; McMahon, B.; Nienhaus, G. U.; Young, R. D. *Biophys. J.* **1996**, *71*, 1563−1573.
(75) Olson, J. S.; Soman, J.; Phillips, G. N., Jr. *IUBMB Life* **2007**, *59*, 552−562.
(76) Scott, E. E.; Gibson, Q. H.; Olson, J. S. *J. Biol. Chem.* **2001**, *276*, 5177−5188.
(77) Olson, J. S.; Mathews, A. J.; Rohlfs, R. J.; Springer, B. A.; Egeberg, K. D.; Sligar, S. G.; Tame, J.; Renaud, J. P.; Nagai, K. *Nature* **1988**, *336*, 265−266.
(78) Pesce, A.; Nardini, M.; Dewilde, S.; Capece, L.; Marti, M. A.; Congia, S.; Salter, M. D.; Blouin, G. C.; Estrin, D. A.; Ascenzi, P.; et al. *J. Biol. Chem.* **2011**, *286*, 5347−5358.
(79) Srajer, V.; Reinisch, L.; Champion, P. M. *Biochemistry* **1991**, *30*, 4886−4895.